Aalborg Universitet

High frequency resonance in DFIG-based wind farm with variable power capacity

Song, Yipeng; Nian, Heng; Blaabjerg, Frede

High Frequency Resonance in DFIG-Based Wind Farm with Variable Power Capacity

Yipeng Song[1]*, Heng Nian[2], and Frede Blaabjerg[1]

(1. Department of Energy Technology, Aalborg University, Aalborg East 9220, Denmark;

2. College of Electrical Engineering, Zhejiang University, Hangzhou, 310027, China)

Abstract: As wind power penetration has been gaining in the power grid for decades, a large number of the doubly fed induction generator(DFIG) based wind farms are being established around the globe. The power capacities of these wind farms may vary around hundreds of MW, and most of the wind farms are connected to long transmission cables whose impedances can not be ignored and require careful attention. Several works have investigated the impedance interaction between the DFIG based wind farm and long transmission cables which may unfortunately cause high frequency resonance (HFR). The main contribution of this paper is to investigate the influence of the variable wind farm capacity on the behavior of the HFR when certain transmission cables are provided. It is found out that the potential HFR may happen in certain wind farms, and the larger wind farm capacity causes more severe HFR due to the relatively weaker grid transmission capability. Simulation results based on Matlab/Simulink are given to validate the analysis of HFR.

Keywords: DFIG based wind farm, variable power capacity, long transmission cable, high frequency resonance.

1 Introduction

The recent rapid growth of renewable power generation has been reported all over the world. Among the several different renewable power sources, wind power generation is one of the most promising solutions[1-3]. From the early year of 21st century, the doubly fed induction generator(DFIG) based wind farm has drawn increasing attention from commercial companies as well as the scientific researchers.

Often the grid voltage of the wind farm is not ideal, but is subject to detrimental operational conditions such as grid voltage three-phase unbalance and harmonics distortion, three-/single- phase voltage fault, as well as frequency deviation. In order to deal with these problems, several enhanced control strategies have been implemented regarding grid voltage fault[4], three-phase unbalance[5-6], harmonic distortion[7-8], as well as for the special topology of connection to the dc voltage grid[9].

Normally, the DFIG based wind farm delivers renewable power to the main grid via the long transmission cables. As reported previously, the cable impedance of the long transmission cable is relatively larger than the conventional stiff grid[10-12], thus the wind farm is often under the operational condition of weak grid due to the large cable impedance.

In the discussion of this paper, the impedance modeling of the long transmission cable is assumed to be a series connection of several Π units[12], where there is a cable resistance and a cable inductance in series connection, and two cable shunt capacitances at both ends[10-12] in each single Π unit. On the other hand, the DFIG based wind farm behave mostly

inductive in the control frequency range[13-16]. Due to their respective inductive and capacitive behaviors, a resonance may happen as a consequence of the impedance interaction between the wind farm and the transmission cable, which will be explained in detail.

HFR analysis has been conducted in [13-16], where several influencing factors are considered, i.e., different parameters of the long transmission cable, different parameters of single DFIG system unit, variable rotor speed, variable output power. Moreover, the active damping strategies were also proposed in [14-16] to mitigate the HFR and ensure safe and reliable operation of the DFIG system.

Nevertheless, the power capacity of the DFIG based wind farm is always set constant in the previous discussions[13-16]. Practically, the power capacity of the commercial wind farms may vary within a wide range around the globe due to different climate conditions, local grid transmission capability and economic concerns. Thus, it is necessary to discuss the HFR under the condition of variable power capacity of the DFIG based wind farm.

This paper is organized as following: the impedance modeling of a single DFIG system unit as well as the wind farm is established in Section 2. Then, the impedance modeling of the Π units based long transmission cable is established in Section 3. Thereafter, the HFR can be analyzed on the basis of the obtained impedance modeling of both the wind farm and the cable in Section 4. Note that, several case studies with different power capacity of the wind farm will be analyzed in this section, and the relationship between the occurrence of HFR and the wind farm power capacity can be obtained. Finally, the simulation results by Matlab/Simulink are provided in Section V in order to verify the analysis of the HFR.

---

* Corresponding Author, E-mail: yis@et.aau.dk.

2   Impedance modeling of the wind farm

This section firstly introduces the diagram of the DFIG based wind farm connected to the transmission cables in Fig.1, where then the impedance modeling of the wind farm can be deduced.

2.1   Introduction to the wind farm and the cable

Fig.1 shows the diagram of the DFIG based wind farm connected to the long transmission cable. Each single DFIG unit includes two parts: 1) the RSC and the DFIG generator; 2) the GSC and the output LCL filter. The parameters of the DFIG unit are shown in Table 1. The three-terminal transformer T_1 is adopted to adjust the output voltage to 690 V.

The transformer T_2 is implemented to increase the voltage level up to 33kV in order to connect each single DFIG unit to the 33kV common AC bus. The impedance of the 33kV transmission cable is neglected due to its relatively shorter length compared with the 150kV cable.

After collecting the wind power at 33kV AC bus, the voltage level is again increased up to 150kV through the transformer T_3. The 150kV long transmission cable is assumed to be modeled as multiple Π units in series. Each Π unit includes the cable resistor R_1 and the cable inductor L_1 in series connection and the cable shunt capacitor $C_1/2$ at both ends.

2.2   Impedance modeling of the DFIG based wind farm

Before deducing the impedance modeling of the DFIG based wind farm, it is necessary to first obtain the impedance modeling of the single DFIG unit, which includes both the RSC and the DFIG generator, as well as the GSC and the output LCL filter[13-16] as following.

The grid part of the DFIG system contains the GSC and the LCL filter, and its impedance modeling in the stationary frame shown in Fig.2 can be obtained[13-16],
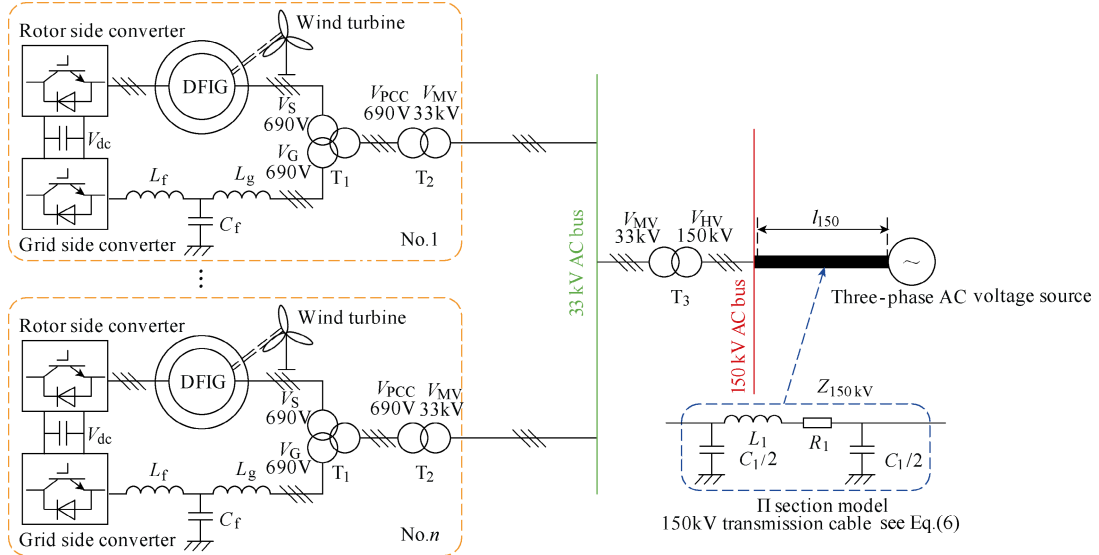
Fig.1   Diagram of the DFIG based wind farm with multiple wind turbines connected to a long transmission cable

Table 1   Parameters of 2MW DFIG units and long transmission cables

| Parameters	Value	Parameters	Value
DFIG generator			
Rated power/MW	2	T_d/μs	300
R_s/Ω	0.0015	R_r/Ω	0.0016
$L_{\sigma s}$/ mH	0.04	$L_{\sigma r}$/mH	0.06
L_m/mH	3	Pole pairs	3
f_s/kHz	5	f_{sw}/kHz	2.5
LCL filter			
L_g/μH	125	L_f/μH	125
C_f/ μF	220		
Current controller parameters in RSC and GSC			
K_{prsc}	0.08	K_{irsc}	2
K_{pgsc}	0.08	K_{igsc}	2
Voltage level			
V_G/V	690	V_{SR}/V	690
V_{PCC}/V	690	V_{MV}/kV	33
V_{HV}/kV	150		
Transmission cable			
L_0/ (mH/km)	0.4	R_0/ (mΩ/km)	25
C_0/(μF/km)	0.14		
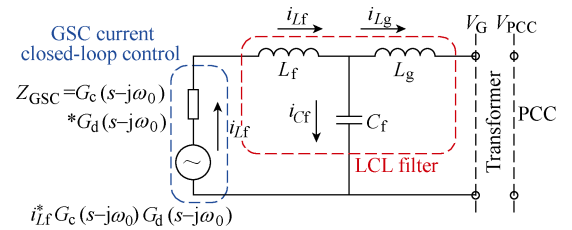
Fig.2   Impedance modeling of the grid side converter (GSC) with LCL filter

$$Z_G = K_1^2 \frac{Z_{Cf}(Z_{Lf}+Z_{GSC})+Z_{Lg}(Z_{Lf}+Z_{GSC})+Z_{Cf}Z_{Lg}}{Z_{Cf}+(Z_{Lf}+Z_{GSC})}$$

(1)

where, $Z_{Cf}=1/sC_f$, $Z_{Lf}=sL_f$, $Z_{Lg}=sL_g$. C_f is the LCL-filter capacitance, L_f is the converter side inductance, and L_g is the LCL grid side inductance. K_1 is the voltage ratio between V_G and V_{PCC} defined as $K_1 = V_{PCC}/V_G$. $Z_{GSC} = G_c(s-j\omega_0)G_d(s-j\omega_0)$, $G_c(s-j\omega_0)$ is the PI current controller containing the proportional

part K_{pgsc} and the integral part $K_{igsc}/(s-j\omega_0)$, the parameters of K_{pgsc} and K_{igsc} are given in Table 1. $G_d(s-j\omega_0)$ is the digital control delay of 1.5 sample period caused by the sampling and PWM update[13-16]. ω_0 is the grid fundamental angular speed of 100π rad/s, it is introduced to represent the rotation from the stationary to the synchronous frame. The control of the DC-link voltage and the grid synchronization in the GSC are neglected due to the slower dynamic response[13-16].

The impedance of the RSC and DFIG generator in the stationary frame can be obtained in Fig.3 as [13-16],

$$Z_{SR} = K_2^2 \frac{Z_{Lm}H + (R_s + Z_{L\sigma s})H + Z_{Lm}(R_s + Z_{L\sigma s})}{Z_{Lm} + H} \quad (2)$$

where $H = Z_{L\sigma r} + (R_r + Z_{RSC})/\text{slip}$; $Z_{RSC} = G_c(s-j\omega_0)G_d(s-j\omega_0)$, $Z_{Lm} = sL_m$; $Z_{L\sigma r} = sL_{\sigma r}$; $Z_{L\sigma s} = sL_{\sigma s}$. R_r is the rotor resistance, L_m is the mutual inductance, $L_{\sigma r}$ is the rotor leakage inductance, and $L_{\sigma s}$ is the stator leakage inductance. K_2 is the voltage ratio between V_S and V_{PCC} as defined $K_2 = V_{PCC}/V_S$. The rotor current control is implemented in the synchronous reference frame, and needs to be rotated to the rotor stationary frame using the slip angular speed expressed as [13-16],

$$\text{slip} = \frac{s - j\omega_r}{s} \quad (3)$$

where, ω_r is the rotor angular speed.

Since the RSC and DFIG generator Z_{SR} and the GSC and LCL-filter Z_G are connected in parallel, the impedance of the single DFIG unit Z_{single} can be obtained based on (1) and (2) as,

$$Z_{single} = K_3^2 \frac{Z_G Z_{SR}}{Z_G + Z_{SR}} \quad (4)$$

where, $K_3 = V_{MV}/V_{PCC}$.

Since it is appropriate and reasonable to assume that all the DFIG units in the wind farm are working in the same conditions, it is assumed in this paper that all the single DFIG units are identical with same parameters, and thus the impedance of the wind farm can be calculated by dividing the impedance of the single DFIG unit with the number of units n_{DFIG} as following.

$$Z_{farm} = \frac{Z_{single}}{n_{DFIG}} \quad (5)$$

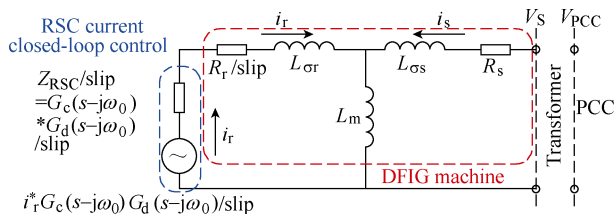where, n_{DFIG} is the number of DFIG units.

Fig.3   Impedance modeling of the DFIG generator and the rotor side converter (RSC)

3   Impedance modeling of the cable

The modeling of the transmission cable has been investigated in [12] and the Π unit based cable modeling is a common solution which is shown in Fig.4.

As can be seen, the Π unit contains the cable resistance R_1 and inductance L_1 in series connection, and the shunt capacitance $C_1/2$ between the cable and the ground. Note that R_1, L_1 and C_1 are the cable parameters of each single Π unit, and the length of each single Π unit l_{single} needs to be taken into consideration as following.

$$R_1 = l_{single}R_0; L_1 = l_{single}L_0; C_1 = l_{single}C_0 \quad (6)$$

where, R_0, L_0 and C_0 are the per km resistance, inductance and capacitance as given in Table 1.

Then, the impedance modeling of the long cable with n Π units can be expressed as,

$$\begin{cases} Z_{unit(1)} = \dfrac{1}{K_4^2}\left(Z_p + \dfrac{1}{Y_p + 1/Z_p}\right) & n = 1 \\[3mm] Z_{unit(n)} = \dfrac{1}{K_4^2}\left(Z_p + \dfrac{1}{Y_p + 1/Z_{unit(n-1)}}\right) & n < \text{unit number} \\[3mm] Z_{unit(n)} = \dfrac{1}{K_4^2}\dfrac{1}{Y_p/2 + 1/Z_{unit(n-1)}} & n = \text{unit number} \end{cases}$$

$$\quad (7a)$$

$$Z_p = sL_1 + R_1; \quad Y_p = 1/(sC_1) \quad (7b)$$

where, n is the number of Π units. $K_4 = V_{HV}/V_{MV}$ is the voltage ratio between the high voltage $V_{HV} = 150$ kV and the medium voltage $V_{MV} = 33$ kV.

Fig.5 shows the Bode diagram of the impedance modeling of the transmission cable with multiple Π units $n = 8, 10, 12$, $l_{single} = 5$km (total length = 40, 50, 60km). According to [10], the length of the single unit l_{single} is appropriately chosen as 5km, as this value makes a reasonable compromise between the cable modeling complexity and accuracy.
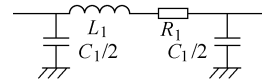

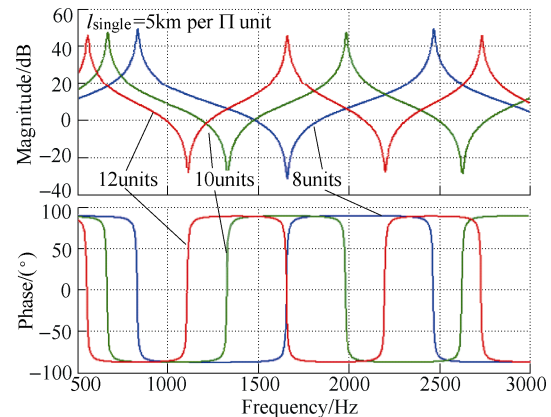Fig.4   Π unit based modeling of the long transmission cable

Fig.5   Bode diagram of the impedance modeling of the transmission cable with multiple Π units $n = 8, 10, 12$, $l_{single} = 5$km (total length = 40km, 50km, 60km)

As shown in Fig.5, as the transmission cable becomes longer, the magnitude peak moves towards lower frequency. Moreover, the potential resonance frequency range, where the phase response of the cable is −90°, also moves towards lower frequency range as the cable becomes longer. For instance, for the case of n = 10 in green, the potential resonance frequency (phase = −90°) is from 2000Hz to 2600Hz; while for the case of n =12 unit in red, the potential resonance frequency (phase = −90°) shifts to lower as from 1700Hz to 2200Hz.

4   Analysis of HFR in wind farms

Based on the impedance modeling of both the DFIG based wind farm and the long cable obtained above, the HFR can be analyzed on the basis of the Bode diagram analysis method.

Note that due to the limited space in this paper, the following discussion of HFR will be conducted with a constant cable length of 60km (n = 12 Π units), while the power capacity of the wind farm may vary as 300MW (n_{DFIG} = 150), 400MW (n_{DFIG} = 200) and 500MW (n_{DFIG} = 250) respectively, which is possible in the practical commercial wind farm around the globe.
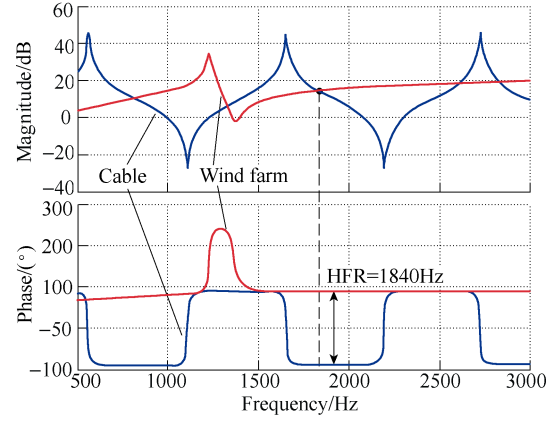
Fig.6 shows the Bode diagram of the impedance of the 60km 150kV transmission cable and the impedance of the DFIG based wind farm with the capacity of (a) 300MW (n_{DFIG} = 150); (b) 400MW (n_{DFIG} = 200); (c) 500MW (n_{DFIG} = 250).
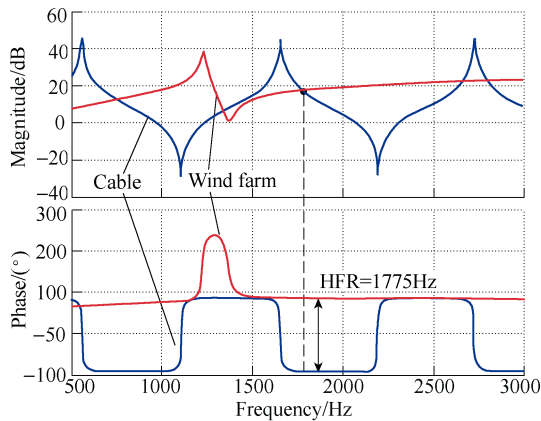
(a) 300MW (n_{DFIG} = 150) DFIG based wind farm
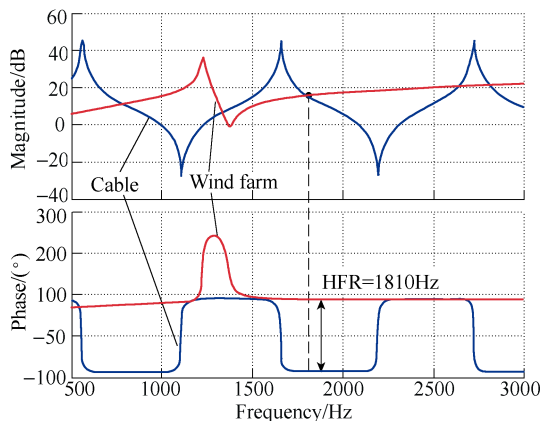
(b) 400MW (n_{DFIG} = 200) DFIG based wind farm

(c) 500MW (n_{DFIG} = 250) DFIG based wind farm

Fig.6   Bode diagram of the impedance of the 60km 150kV transmission cable and the impedance of the DFIG based wind farm with different power capacity

By comparing the impedance of the wind farm with three different power capacities (red curves in the three Bode diagrams), it can be found out that its magnitude response drops as the capacity increases, which is due to the increasing number of DFIG units working in parallel, while the phase response remains constant regardless of the different power capacity.

On the other hand, in each of these three cases, the magnitude intersection point exists at 1775Hz with 300MW wind farm in Fig.6(a), 1810Hz with 400MW wind farm in Fig.6(b), and 1840Hz with 500MW wind farm in Fig.6(c). The phase differences between the cable and the wind farm are all 180° in these three cases, thus the HFRs at 1775Hz, 1810Hz and 1840Hz occur consequently for the three case studies. Note that although additional magnitude intersection points exist at other frequencies, the phase difference at these frequencies are smaller than 180°, thus no HFR will occur at these frequencies.

5   Simulation validation

5.1   Simulation setup

In order to validate the HFR in the wind farm, a simulation model is built where the control block is shown in Fig.7 and the DFIG system parameters can be found in Table 1. The transmission cables are simulated as shown in Fig.1 with their parameters listed in Table 1. The rotor speed is set to 1200r/min (0.8pu), with the synchronous speed of 1500r/min(1.0pu). The DC-link voltage is 1200V. The switching frequency f_{sw} for both RSC and GSC is 2.5kHz, the sampling frequency f_s for both RSC and GSC is 5kHz. The output wind power is set as 1.0pu active power and 0.0pu reactive power.

Clearly it is impossible to run the simulation based on Mablab/Simulink with 200 single DFIG units whose power capacity is 2MW each, two single DFIG units are adopted here, while the impedance of the transmission cables are multiplied with 75, 100, 125 in simulation in order to represent the total number of n_{DFIG} = 150, 200, 250 DFIG units, which finally build up a 300MW, 400MW, 500 MW wind farm.
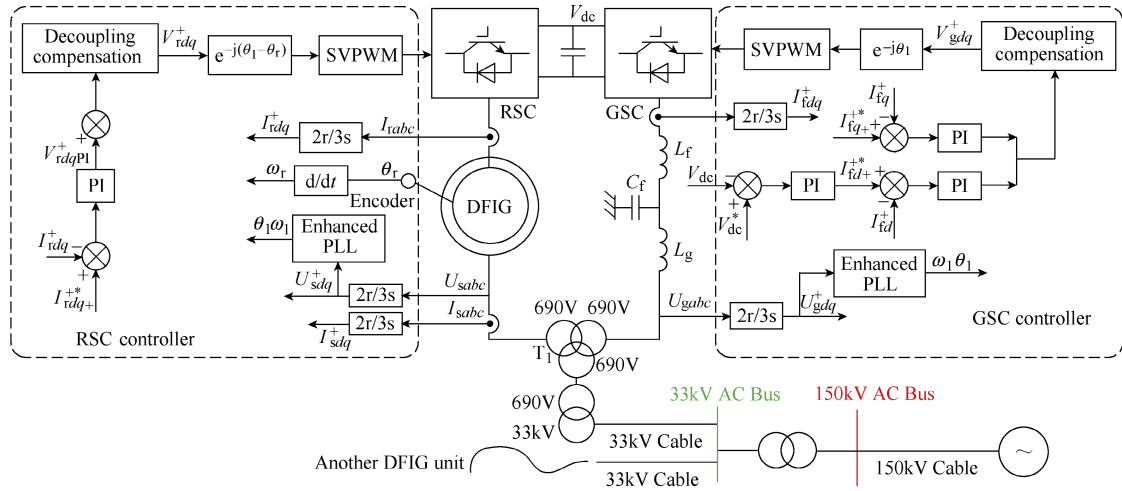
Fig.7   Control block diagram of a single DFIG unit including the connection to the grid through long transmission cables

5.2   Control block diagram

Fig.7 shows the control block diagram of a single DFIG unit connecting to the grid through long transmission cables. As can be seen, for the RSC control, an Enhanced Phase Locked Loop (EPLL) is used to obtain the grid voltage fundamental synchronous angular speed ω_1 and angle θ_1, while an encoder gives out the DFIG rotor position θ_r and speed ω_r. The rotor current $I^+ rdq$ is first sampled and then controlled based on the reference value $I^{+*} rdq$ with a PI controller to output the harvested wind energy. The output of the rotor current PI closed-loop control $V^+ rdq$PI are added together with the decoupling compensation, giving out the rotor control voltage $V^+ rdq$, it is then transformed to the rotor stationary frame as the input to the Space Vector Pulse Width Modulation (SVPWM).

As for the GSC control, the dc-link voltage V_{dc} is well regulated by a PI controller, and its output is delivered as the converter side inductance filter current reference $I^{+*} fdq$, which is used to regulate the actual converter side inductance filter current $I^+ fdq$ by a PI controller. Similarly, the GSC control voltage $V^+ gdq$ can be obtained by the PI current controller output and the decoupling compensation.
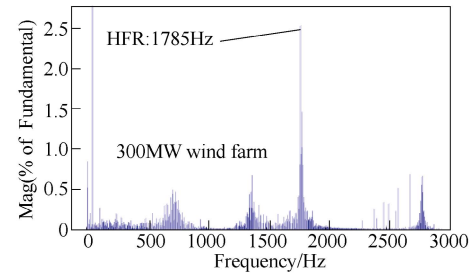
5.3   Simulation results

Fig.8~Fig.10 give the simulation results of the DFIG based wind farm with different power capacity of 300MW in Fig.8, 400MW in Fig.9 and 500 MW in Fig.10. The transmission cable is set constant as 60km with $n = 12$.

As can be observed from the simulation results in Fig.8~Fig.10, the three cases all contain the HFR components in the DFIG system performance. That is, 1) For the case of 300MW wind farm, analysis HFR = 1775Hz in Fig.6(a), simulation HFR=1785Hz in Fig.8; 2) For the case of 400MW wind farm, analysis HFR = 1810 Hz in Fig.6(b), simulation HFR=1820Hz in Fig.9; 3) For the case of 500MW wind farm, analysis HFR = 1840Hz in Fig.6(c), simulation HFR=1850Hz in Fig.10;

Table 2 summarizes the analysis and simulation results of the HFR, and it can be found that the analysis
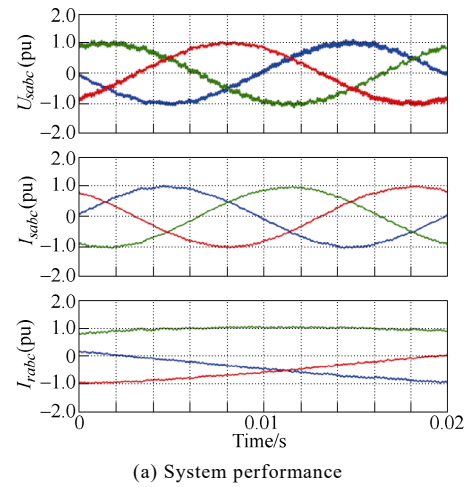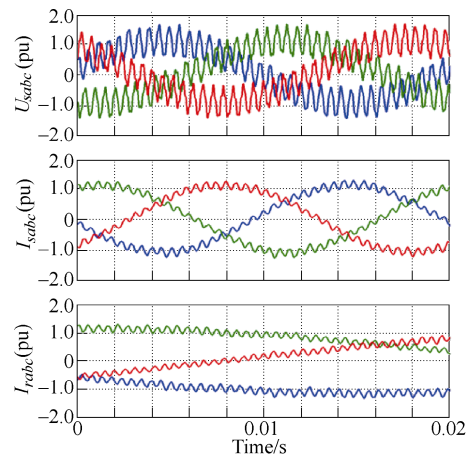

(a) System performance

(b) Stator voltage FFT analysis

Fig.8   Simulation results of 300MW DFIG based wind farm and the cable length = 60km
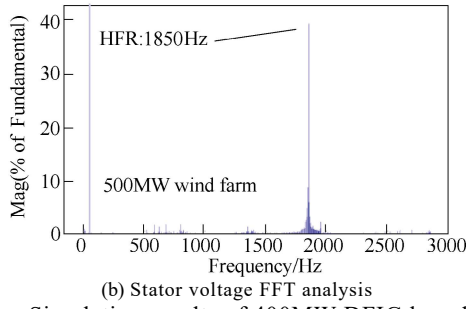

(a) System performance

(b) Stator voltage FFT analysis

Fig.9   Simulation results of 400MW DFIG based wind farm and the cable length = 60km

(a) System performance
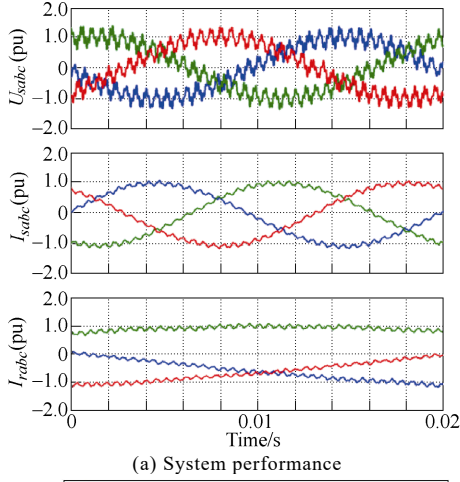

(b) Stator voltage FFT analysis

Fig.10   Simulation results of 500MW DFIG based wind farm and the cable length = 60km

Table 2   Analysis and simulation results of HFR in DFIG based wind farm

	Wind farm capacity/MW		
	300	400	500
Analysis HFR/Hz	1775	1810	1840
Simulation HFR/Hz	1785	1820	1850

results of HFR match well with the simulation results, thus the HFR in the DFIG based wind farm can be validated.

6   Conclusion

This paper has investigated the HFR phenomenon in the DFIG based wind farm connected to the long transmission cable. The long cable is modeled as multiple Π units in series, including the cable resistor and inductor in series connection and the shunt capacitor at both ends. Several conclusions can be obtained.

(1) The Bode diagram based analysis method can be adopted to theoretically explain the principle of the HFR, and simulation results are provided to validate

the HFR.

(2) The larger power capacity of the DFIG based wind farm results in slightly higher HFR frequency due to its smaller magnitude caused by the larger number of DFIG units.

(3) From the perspective of grid impedance weakness, it can be found that the weaker grid transmission capability (i.e., larger impedance of the long cable) results in the severer HFR phenomenon. For instance, the relatively small capacity 300MW of the wind farm causes small amount of HFR, while the relatively large capacity 500MW of the wind farm causes significant HFR.

References

[1] F. Blaabjerg, and K. Ma, "Future on power electronics for wind turbine systems," *IEEE J. Emer. Sel. Topics Power Electron.*, vol. 1, no. 3, pp. 139-152, Sep. 2013.

[2] K. Ma, L. Tutelea, I. Boldea, D. M. Ionel, and F. Blaabjerg, "Power electronic drives, controls, and electric generators for large wind turbines–an overview," *Electric Power Components and Systems*, vol. 43, no. 12, pp. 1406-1421, 2015.

[3] V. Yaramasu, B. Wu, P. C. Sen, S. Kouro, and M. Narimani, "High-power wind energy conversion systems: State-of-the-art and emerging technologies," *Proceedings of the IEEE*, vol. 103, no. 5, pp. 740-788, 2015.

[4] J. Hu, B. Wang, W. Wang, H. Tang, Y. Chi, and Q. Hu. "Small signal dynamics of DFIG-based wind turbines during riding through symmetrical faults in weak AC grid," *IEEE Trans. Energy Convers.*, accepted & in press.

[5] H. Nian, P. Cheng, and Z. Q. Zhu, "Independent operation of DFIG-based WECS using resonant feedback compensators under unbalanced grid voltage conditions," *IEEE Trans. Power Electron.*, vol. 30, no. 7, pp. 3650-3661, July 2015.

[6] H. Nian, P. Cheng, and Z. Q. Zhu, "Coordinated direct power control of DFIG system without phase-locked loop under unbalanced grid voltage conditions," *IEEE Trans. Power Electron.*, vol. 31, no. 4, pp. 2905-2918, Apr. 2016.

[7] C. Wu, and H. Nian, "Stator harmonic currents suppression for DFIG based on feed-forward regulator under distorted grid voltage," *IEEE Trans. Power Electron.*, accepted.

[8] C. Chen, and H. Nian, "Low-complexity model predictive stator current control of DFIG under harmonic grid voltages," *IEEE Trans. Energy Convers.*, accepted & in press.

[9] H. Nian, C. Wu, and P. Cheng, "Direct resonant control strategy for torque ripple mitigation of DFIG connected to DC link through diode rectifier on stator," *IEEE Trans. Power Electron.*, accepted.

[10] M. Zubiaga, G. Abad, J. A. Barrena, S. Aurtenetxea, and A. Cárcar, "Spectral analysis of a transmission system based on AC submarine cables for an offshore wind farm," in *Proc. of Annual Conference of IEEE Industrial Electronics (IECON)*, Nov. 3-5, 2009.

[11] H. Zhang, G. François, F. Diana, and S. Christophe, "Analysis of the influence of different cable modelling for DC series offshore wind farm," in *Proc. of Power Electronics and Applications (EPE'16 ECCE Europe)*, Sept. 5-9, 2016.

[12] Z. Chen, A. Luo, H. Kuang, L. Zhou, Y. Chen, and Y. Huang, "Harmonic resonance characteristics of large-scale distributed power plant in wideband frequency domain," *Electric Power Systems Research*, vol. 143, pp. 53-65, 2017.

[13] Y. Song, X. Wang, and F. Blaabjerg, "Impedance-based high frequency resonance analysis of DFIG system in weak grids," *IEEE Trans. Power Electron.*, vol. 32, no. 5, pp. 3536-3548, May 2017.

[14] Y. Song, F. Blaabjerg, and X. Wang, "Analysis and active damping of multiple high frequency resonances in DFIG system," *IEEE Trans. Energy Convers.*, vol. 32, no. 1, pp. 369-381, March 2017.

[15] Y. Song, X. Wang, and F. Blaabjerg, "High frequency resonance damping of DFIG based wind power system under weak network," *IEEE Trans. Power Electron.*, vol. 32, no. 3, pp. 1927-1940, Mar. 2017.

[16] Y. Song, and F. Blaabjerg, "Wide frequency band active

damping strategy for DFIG system high frequency resonance," *IEEE Trans. Energy., Convers.*, vol. 31, no. 4, pp. 1665-1675, Dec. 2016.
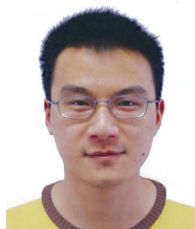
Yipeng Song was born in Hangzhou, China. He received the B.Sc. degree and Ph.D. degree both from the College of Electrical Engineering, Zhejiang University, Hangzhou, China, in 2010 and 2015. He is currently working as a Postdoc at the Department of Energy Technology in Aalborg University, Denmark. His current research interests are motor control with power electronics devices in renewable-energy conversion, particularly the control and operation of doubly fed induction generators for wind power generation.

Heng Nian received the B.Eng. degree and the M.Eng. degree from HeFei University of Technology, China, and the Ph.D. degree from Zhejiang University, China, in 1999, 2002, and 2005 respectively, all in electrical engineering. From 2005 to 2007, he was as a Post-Doctoral with the College of Electrical Engineering, Zhejiang University, China.

In 2007, he was promoted as an Associate professor. Since 2016, he has been a Full Professor at the College of Electrical Engineering, Zhejiang University, China. From 2013 to 2014, he was a visiting scholar at the Department of Electrical, Computer, and System Engineering, Rensselaer Polytechnic Institute, Troy, NY. His current research interests include the optimal design and operation control for wind power generation system. He has published more than 20 IEEE/IET Transaction papers and holds more than 20 issued/pending patents.

Frede Blaabjerg was with ABB-Scandia, Randers, Denmark, from 1987 to 1988. From 1988 to 1992, he was a Ph.D. Student with Aalborg University, Aalborg, Denmark. He became an Assistant Professor in 1992, Associate Professor in 1996, and Full Professor of power electronics and drives in 1998. His current research interests include power electronics and its applications such as in wind turbines, PV systems, reliability, harmonics and adjustable speed drives.

He has received 17 IEEE Prize Paper Awards, the IEEE PELS Distinguished Service Award in 2009, the EPE-PEMC Council Award in 2010, the IEEE William E. Newell Power Electronics Award 2014 and the Villum Kann Rasmussen Research Award 2014. He was an Editor-in-Chief of the IEEE TRANSACTIONS ON POWER ELECTRONICS from 2006 to 2012. He is nominated in 2014 and 2015 by Thomson Reuters to be between the most 250 cited researchers in Engineering in the world.